A regularized reconstruction pipeline for high-definition diffusion MRI in challenging regions incorporating a per-shot image correction

A regularized reconstruction pipeline for high definition diffusion MRI in challenging regions incorporating a per-shot image correction

Samuel F. Cousin[§], Gilad Liberman[§], Eddy Solomon, Martins Otikovs, Lucio Frydman*

Department of Chemical and Biological Physics, Weizmann Institute, 7610001 Rehovot, Israel

[§] These two authors contributed equally to this work.

Keywords: spatiotemporal encoding (SPEN), interleaved acquisitions, inter-scan correction, regularized reconstruction, brain DTI

Abbreviations: DTI, Diffusion Tensor Imaging; DWI, Diffusion Weighted Imaging; EPI, Echo-Planar Imaging; FOV, Field of View; FT, Fourier Transform; MRI, Magnetic Resonance Imaging; RF, Radio frequency; RO, Readout; SE, Spin-Echo; SNR, Signal-to-Noise Ratio; SPEN, Spatiotemporal Encoding; TE, Echo Time; TR, Repetition Time

Running Title: *Human DTI at sub-mm resolution in challenging regions*

Figures and Tables: 5 Figures in main text; 5 in the Supporting Information

Equations count: 0

References count: 48

Word count: 2393

*Prof. Lucio Frydman; +972-8-9344903; lucio.frydman@weizmann.ac.il

Abstract

Purpose: Diffusion MRI is of interest for clinical research and diagnosis. While high resolution DWI/DTI is hard to achieve by single-shot methods, interleaved acquisitions can deliver these – provided motion and/or folding artefacts are overcome. Thanks to its ability to provide zoomed, folding-free images, SPatially ENcoded (SPEN) MRI can fulfil these requirements. This was coupled with a regularized reconstruction and parallel receive methods, to deliver a robust scheme for human DWI/DTI at mm and sub-mm resolutions.

Methods: Each shot along the SPEN dimension was reconstructed separately to retrieve per-shot phase maps. These, together with coil sensitivities, were combined with SPEN's quadratic phase encoding matrices associated to each shot into single global operators. Their originating images were then iteratively computed aided by l1 and l2 regularisation methods. When needed, motion-corrupted shots were discarded and replaced by redundant information arising from parallel imaging.

Results: Full brain DTI experiments at 1 mm and restricted brain DTIs with 0.75mm nominal in-plane resolutions were acquired and reconstructed successfully by the new scheme. These 3T SPEN results compared favourably with EPI counterparts, based on segmented and selective excitation schemes provided with the scanner.

Conclusions: A new procedure for achieving high definition diffusion-based MRI was developed and demonstrated.

INTRODUCTION

Diffusion imaging is of major clinical and research interests,[1] with applications including tumour detection,[2] stroke characterization[3] and connectomics[4]. Thanks to their independence from unavoidable inter-scan motional effects, single-shot techniques like EPI are usually needed to map the µm-size motions being sought in quantitative diffusion measurements. While resolution and robustness to field inhomogeneities are limited in single-shot EPI, multi-shot interleaving can be used for improving these images quality. In diffusion measurements, however, each shot will be impacted by spatially-dependent phases, arising from interferences between collective motions and the diffusion sensitizing gradients[5]. Many successful attempts have been made to reduce these motion artefacts, and reach millimetre or submillimetre resolution with diffusion experiments. Some of these techniques use navigators to acquire separately the per-shot phase changes.[6,7] Others (SNAILS,[8] keyhole,[9] PROPELLER,[10] RESOLVE[11]) use different acquisition trajectories which repeatedly cover certain regions of k-space, to deduce from these redundancies the phase corrections that should be used to compensate the motions occurring between different shots. Using multi-receiver head-coil, parallel imaging methods that can deduce complementary *k*-space regions, have also been used to solve motion artefacts;[12,13] some have also led to impressive 3D DTI reconstructions.[14,15]

SPatiotemporal ENcoding (SPEN) is a single-shot MRI technique which excites the spins and rasterizes the image profile in a spatially sequential manner, rather than acquiring equal-amplitude *k*-domain signals from all spins simultaneously.[16–23] SPEN's resolution is largely defined at excitation rather than at acquisition, allowing one to use stronger phase-encoding acquisition gradients than in EPI. This imparts higher robustness against inhomogeneity-induced distortions, at the expense of compromises in power deposition (SAR) and single-to-noise ratio (SNR). SPEN's Field-of-View (FOV) is also defined before the acquisition by a swept encoding pulse, leading to a quadratic spin evolution phase that can avoid folding artefacts even upon zooming along the "low-bandwidth" (SPEN) axis. By contrast to what occurs in interleaved EPI,[24] subsampling this axis during acquisition therefore does not bring about image folding effects:[25] it only leads to lower resolution SPEN images. If available, resolution can then be improved by relying on multiple-coil information –which then provides missing data in the spatial rather than in the usual *k*-domain.[26] Alternatively, resolution can be improved by collecting multiple interleaved shots, where each shot will lead to full FOV images involving separate, slightly spatially shifted information. An additional characteristic worth remarking for these experiments rests in their ability to lead to sequential echoes throughout the course of the

signal acquisition rather than at a single TE echo time; this kind of "full refocusing" further frees the ensuing images from potential T2* effects throughout the course of the acquisition.

Despite the potential of these experiments, a relatively long acquisition readout (RO) train depending on this gradient slew rate and strength, ends up limiting the actual resolution of single-scan SPEN MRI. As mentioned, this can be improved by the use of data interleaving.[25] When implemented within the context of diffusion MR experiments, however, such multi-shot acquisitions call for care, as they need to deal with the systematic and the random shot-specific motions, that invariable take place in *in vivo* experiments. Due to the bipolar gradients involved in diffusion-weighting experiments, this will affect the image outcome in a shot-specific way and lead to sizable artefacts. This work introduces a robust reconstruction procedure for the recovery of high-resolution diffusion data in such multi-shot, interleaved SPEN experiments. The procedure exploits the aforementioned advantages of SPEN, including the fact that the phase of each single-shot image can be extracted without navigators, and that zooming is possible without folding complications. Redundancy available from parallel receiving setups, as well as image domain regularization methods based on the BART toolbox,[27,28] were also incorporated. Quality diffusion-weighted images on clinical settings could thus be obtained; we exploit this to implement sub-mm diffusion-weighted and diffusion-tensor imaging experiments targeting deep human brain regions on a commercial 3T clinical platform.

METHODS

All experiments were approved by the Internal Review Boards of Wolfson Medical Center (WOMC-0091-11, Holon, Israel) and of the Weizmann Institute, and were collected after obtaining suitable informed consents. Human volunteers were scanned on 3T Siemens TimTRIO® and Prisma® platforms (Erlangen, Germany), using 32-channel and 20-channel head coils respectively. The acquisition schemes were modelled on the fully refocused interleaved SPEN procedures of Schmidt,[25] Liberman[26] et al., but endowed with a new reconstruction scheme that incorporates both per-shot as well as global phase corrections. The main features of this novel scheme are presented in Figure 1, as pertaining to the acquisition of diffusion-oriented experiments. This scheme is separated into a series of distinct processes, including: (i) combination of the multi-receive b_0 data into one channel using the geometrical coil compression algorithm[29] (GCC, implemented so as to keep the signal intensity losses to ≤5%), and separation of the multi-shot sets into two sets corresponding to acquisitions performed under positive/negative readout acquisition gradients (also referred to as the even-odd

data sets); (ii) reconstruction of the even and odd b_0 images and determination of the subsequent even/odd phase correction via linear fittings along the readout dimensions; (iii) application of these even/odd phase corrections to the original multi-channel b_0 and diffusion-weighted data; (iv) reconstruction of each single-shot image and estimation of the relative phases between per-shot images; (v) application of these phase differences to the sensitivity maps determined from the b_0 images, to create unique phase-modulated sensitivity profiles for each shot and for each diffusion-weighted set; and (vi) final reconstruction of the overall image by inverse-analysis of the data arising after step (iii), while incorporating the phase-weighted sensitivity maps and after discarding –if needed– motion-corrupted data sets (as revealed by the relative displacements between each per-shot image).

Steps (ii), (iv) and (vi) above involve obtaining an image out of the experimentally collected data, based on solving an inverse problem that needs to account for the coil sensitivity maps and for the quadratic phase encoding applied as part of the SPEN. Dealing with this quadratic encoding was hitherto done by the super-resolution (SR) procedure,[19,21,25,30–32] which requires knowing the experimental parameters used for the chirp pulse, suitably set according to each interleaved shot acquisition.[25] In the present case BART's Parallel-Imaging-Compressed-Sensing module[27,28] signal model was used to this end, modified by replacing its 2D with a 1D FT procedure along the RO and a multiplication by the SR matrix[33] along the low-bandwidth axis. This inverse solution of the reconstruction problem allowed us to use finite-difference regularization methods;[34–37] several options were tested for performing this optimally, eventually settling for the SparseMRI package[38] relying on a non-linear conjugate gradient (CG) with optional l1 or l2 regularizations (implemented by the ISTA, FISTA and ADMM algorithms). This was found superior to wavelet-based regularizations, as it could better eliminate the striped artefacts otherwise arising in SPEN (the counterpart of the "half-FOV ghosts" arising in k-space techniques). It was found that in these fits l1 regularization helped preserve sharp edges (an assistance that in the images presented below we found unnecessary and hence was not actually used),[39,40] while l2 regularization helped to improve apparent SNR at the expense of imparting a local smoothness.[41–43] (Notice that while for the final reconstructions we used non-linear CG with l2-regularization applied to finite differences, the problem is linear and can in principle be solved using conventional, linear CG methods). Supporting Information Figures S1-S4 assess the impact of different l1 (corresponding to a discrete version of total variation) and l2 weights on final SPEN image reconstruction. Each coil's sensitivity map was obtained based on b_0 data using ESPIRiT,[27,28,44] as applied on a 25x25 central *k*-space patch obtained by inverse FT of the super-

resolved data. Each shot was then used to reconstruct separate full-matrix images by relying on parallel receiving (i.e., on the SUSPENSE approach[26]), while applying a stronger l2 regularization than used for the final image reconstruction (0.2 vs 0.05 for the images presented herein) in order to produce a smoothed phase map free of coil artefacts. These phase mappings were repeated for each shot, and for each diffusion (b-value) repetition. As mentioned, the final reconstruction was then performed by pooling all data sets together, and demanding high-definition maps compatible with all these phase-corrected data; an optional motion screening step was introduced before final reconstruction (see the Supporting Information for its details). Motion-derived striping artefacts could thus be avoided without impacting the final resolution of the image, and only at the expense of a slightly reduced SNR. Finally, from the resulting high-definition diffusion-weighted images, ADC/DTI maps were computed after accounting for the effects of both the imaging and the diffusion gradients onto the b-tensor, along the lines described in Refs. 45,46.

The code for performing this entire SPEN processing pipeline is available for download at https://www.weizmann.ac.il/chemphys/Frydman_group/software.

Image acquisition parameters. Full brain SPEN images were acquired on a Siemens Prisma® scanner using an eight-shot interleaved acquisition, for a final in-plane matrix size of 222x232. Linearly swept encoding pulses with time-bandwidth value of Q=112 and 5 slices were used in the SPEN experiments, for a final resolution of 1x1x3mm. A nominal b-value of 800 s/mm^2 and three diffusion orientations were used in these experiments. Full brain comparisons were carried out against scanner-supplied readout-segmented (RESOLVE) EPI experiments[11], acquired with seven segments leading to a final matrix size of 192x192. The effective bandwidth in the phase-encoding direction of these experiments was 2780 Hz, matching the coverage and slices of the SPEN experiment, and also achieving a final 1x1x3mm nominal resolution. The diffusion weighting used in these EPI scans had a nominal *b*=850 s/mm^2 and also took three diffusion directions. SPEN diffusivity images targeting a restricted FOV centered on the human pons region were also acquired with a Q value of 56 and a matrix size 272x116 using four interleaved shots and 7 slices, for a resolution of 0.72x0.72x3mm. These acquisitions were made on a Siemens TrioTIM® scanner, and compared against the maximum definition that could be obtained in single-shot EPI DTI experiments on the same region: 2x2x3mm (no RESOLVE-like experiment being available for this instrument). These experiments were recorded using 12 diffusion directions and a nominal b=750 s/mm^2 value. Also the chiasma was targeted with this system, in a comparison that used EPI with 2D shaped pulses[47] (ZOOMit) over a FOV of 210x88

mm with 87.5% partial FT sampling along PE direction, and four-shot interleaved SPEN with Q=46, for equal final resolutions of 1x1x3 mm and nominal diffusion values b=850 s/mm^2 with 12 directions.

RESULTS

Figure 2 compares full FOV imaging based on eight interleaved SPEN shots against comparable EPI results obtained using seven readout segments and the RESOLVE algorithm. Shown in this figure are both b0 images corresponding to three similar slices with 1mm in-plane resolutions, as well as their resulting ADC maps. The results of both experiments are comparable, with motion artefacts largely compensated in both cases, as attested by the faithful ADC maps. The signal-to-noise ratio in the SPEN images is slightly lower (≈75%) than in the EPI counterparts due to the larger bandwidths of these experiments. Conversely, this affords the SPEN images with a higher resiliency to magnetic field inhomogeneities than their segmented EPI counterparts, as can be noticed by the more complete absence of pile-up artefacts (arrows).

As mentioned, the pipeline can implement the final image reconstruction utilizing fewer shots than originally planned, using the redundant information available from multiple receivers to maintain resolution at the cost of reduced SNR. Figure 3 summarizes the scan/noise trade off that then happens, as witnessed by the increase in the coil-dependent g-factors for this SUSPENSE-based processing. Avoiding the need to use additional interleaved scans for achieving the desired spatial resolution provides increased immunity to potential motional artefacts; despite this benefit, it is also clear that constant-resolution reconstructions arising from lower numbers of shots increase noise, as attested by the growth in the resulting g-maps.

SPEN's advantages come into play when targeting either inhomogeneity-challenged regions or restricted FOVs. The latter raises challenges to k-based MRI schemes due to the potential presence of folding artifacts. 2D pulses can be used to alleviate such artifacts,[48] an approach that is available in certain scanners. Figure 4 compares DTI results arising from such "ZOOMit®" single shot EPI acquisitions incorporating 2D shaped pulses, versus a multi-shot SPEN-based DTI experiment collected at 1mm in-plane resolution. Targeted in both cases was the optic chiasma region. This sub-brain region is subject to sizable magnetic field inhomogeneities, which create notable pile-ups and voids in the EPI images. Notice as well, on the left-most image of Figure 4, the optic nerves seen in the EPI image –although they belong to other slices not present in the field of view. This stems from inhomogeneity-driven miss-registrations acting during the course of the relatively long 2D RF pulses, phenomena that are not observed in the restricted-FOV SPEN acquisitions.

The per-shot folding-free nature of SPEN enables zooming on regions where parallel imaging information is poor or non-existent. Figure 5 demonstrates this with a DTI analysis of the pons, a relatively small, deep brain structure lying below the cerebellum. EPI data can tackle this region of interest at ca. 2mm in-plane resolution, whereas the protocol in Figure 1 achieves higher details with a nominal 0.74mm in-plane resolution. The higher resolution achieved by SPEN provides details about the fibers inside the pons, enabling the delineation of the pyramidal tract (D1), the oculomotor nerve (CNIII, D3), and the decussation of the medial lemniscus D2 –details that are all lost in the EPI images.

DISCUSSION AND CONCLUSIONS

High-resolution quantitative diffusivity maps have been obtained from multi-shot SPEN experiments, using a novel regularized processing pipeline. These imaging experiments and pipeline explored brain diffusivity for whole-brain scans, where the abilities of various EPI-derived methodologies are well known, as well as under conditions that challenge state-of-the-art EPI due to location and/or problems to achieve high resolution by parallel imaging methods. For the first of these scenarios no clear advantages were noticed for the suggested approach; but for the latter two, SPEN's image-domain nature, its ability to withstand field inhomogeneities and its capacity to zoom into targeted regions, led to superior results. While the final resolution of the reconstruction here introduced depends on the chosen regularization parameters (as demonstrated in the SI), a good compromise can always be found that takes advantage of the regularization and at the same time preserves the nominal resolution. The availability of this regularized reconstruction scheme for interleaved SPEN experiments could open interesting perspectives for the acquisition of high-resolution diffusion images under restricted field of view in other challenging regions, including spine, breast and abdomen. The potential of these avenues is currently under investigation.

ACKNOWLEDGMENTS. We are grateful to Prof. Michael (Miki) Lustig (UC-Berkeley), Dr. Sagit Shushan (Wolfson MC) and Dr. Edna Furman-Haran (Weizmann) for assistance. SFC thanks the Feinberg Graduate School (Weizmann) and the French Foreign Service for partial postdoctoral fellowships. Support came from the Israel Science Foundation (#2508/17), EU ERC-2016-PoC grant # 751106, the Kimmel Institute for Magnetic Resonance and the Perlman Family Foundation.

REFERENCES

1. Mori, S. & Zhang, J. Principles of diffusion tensor imaging and its applications to basic neuroscience research. *Neuron* **51,** 527–539 (2006).

2. Assaf, Y. & Pasternak, O. Diffusion tensor imaging (DTI)-based white matter mapping in brain research: a review. *J. Mol. Neurosci.* **34,** 51–61 (2008).
3. Werring, D. J. *et al.* Diffusion tensor imaging can detect and quantify corticospinal tract degeneration after stroke. *J. Neurol. Neurosurg. Psychiatr.* **69,** 269–272 (2000).
4. Beaulieu, C. The basis of anisotropic water diffusion in the nervous system - a technical review. *NMR Biomed.* **15,** 435–455 (2002).
5. Le Bihan, D., Poupon, C., Amadon, A. & Lethimonnier, F. Artifacts and pitfalls in diffusion MRI. *J. Magn. Reson. Imaging* **24,** 478–488 (2006).
6. Hu, X. & Kim, S. G. Reduction of signal fluctuation in functional MRI using navigator echoes. *Magn. Reson. Med.* **31,** 495–503 (1994).
7. Jeong, E.-K., Kim, S.-E. & Parker, D. L. High-resolution diffusion-weighted 3D MRI, using diffusion-weighted driven-equilibrium (DW-DE) and multishot segmented 3D-SSFP without navigator echoes. *Magn. Reson. Med.* **50,** 821–829 (2003).
8. Liu, C., Bammer, R., Kim, D.-H. & Moseley, M. E. Self-navigated interleaved spiral (SNAILS): application to high-resolution diffusion tensor imaging. *Magn. Reson. Med.* **52,** 1388–1396 (2004).
9. Nunes, R. G., Jezzard, P., Behrens, T. E. J. & Clare, S. Self-navigated multishot echo-planar pulse sequence for high-resolution diffusion-weighted imaging. *Magn. Reson. Med.* **53,** 1474–1478 (2005).
10. Pipe, J. G., Farthing, V. G. & Forbes, K. P. Multishot diffusion-weighted FSE using PROPELLER MRI. *Magn. Reson. Med.* **47,** 42–52 (2002).
11. Porter, D. A. & Heidemann, R. M. High resolution diffusion-weighted imaging using readout-segmented echo-planar imaging, parallel imaging and a two-dimensional navigator-based reacquisition. *Magn. Reson. Med.* **62,** 468–475 (2009).
12. Skare, S. *et al.* Clinical multishot DW-EPI through parallel imaging with considerations of susceptibility, motion, and noise. *Magn. Reson. Med.* **57,** 881–890 (2007).
13. Uecker, M., Karaus, A. & Frahm, J. Inverse reconstruction method for segmented multishot diffusion-weighted MRI with multiple coils. *Magn. Reson. Med.* **62,** 1342–1348 (2009).
14. Chen, N.-K., Guidon, A., Chang, H.-C. & Song, A. W. A robust multi-shot scan strategy for high-resolution diffusion weighted MRI enabled by multiplexed sensitivity-encoding (MUSE). *Neuroimage* **72,** 41–47 (2013).
15. Bruce, I. P., Chang, H.-C., Petty, C., Chen, N.-K. & Song, A. W. 3D-MB-MUSE: A robust 3D multi-slab, multi-band and multi-shot reconstruction approach for ultrahigh resolution diffusion MRI. *Neuroimage* **159,** 46–56 (2017).
16. Tal, A. & Frydman, L. Spectroscopic imaging from spatially-encoded single-scan multidimensional MRI data. *J. Magn. Reson.* **189,** 46–58 (2007).
17. Chamberlain, R. *et al.* RASER: a new ultrafast magnetic resonance imaging method. *Magn. Reson. Med.* **58,** 794–799 (2007).
18. Marhabaie, S., Bodenhausen, G. & Pelupessy, P. Susceptibility contrast by echo shifting in spatially encoded single-scan MRI. *Phys. Chem. Chem. Phys.* **19,** 14210–14213 (2017).
19. Cai, C. *et al.* An efficient de-convolution reconstruction method for spatiotemporal-encoding single-scan 2D MRI. *J. Magn. Reson.* **228,** 136–147 (2013).
20. Li, J. *et al.* Reduced field-of-view imaging for single-shot MRI with an amplitude-modulated

chirp pulse excitation and Fourier transform reconstruction. *Magn. Reson. Imaging* **33,** 503–515 (2015).
21. Li, J. *et al.* Imaging with referenceless distortion correction and flexible regions of interest using single-shot biaxial spatiotemporally encoded MRI. *Neuroimage* **105,** 93–111 (2015).
22. Snyder, A. L. S., Corum, C. A., Moeller, S., Powell, N. J. & Garwood, M. MRI by steering resonance through space. *Magn. Reson. Med.* **72,** 49–58 (2014).
23. Chen, Y. *et al.* Partial Fourier transform reconstruction for single-shot MRI with linear frequency-swept excitation. *Magn. Reson. Med.* **69,** 1326–1336 (2013).
24. Butts, K., Pauly, J., de Crespigny, A. & Moseley, M. Isotropic diffusion-weighted and spiral-navigated interleaved EPI for routine imaging of acute stroke. *Magn. Reson. Med.* **38,** 741–749 (1997).
25. Schmidt, R., Seginer, A. & Frydman, L. Interleaved multishot imaging by spatiotemporal encoding: A fast, self-referenced method for high-definition diffusion and functional MRI. *Magn. Reson. Med.* **75,** 1935–1948 (2016).
26. Liberman, G., Solomon, E., Lustig, M. & Frydman, L. Multiple-coil k-space interpolation enhances resolution in single-shot spatiotemporal MRI. *Magn. Reson. Med.* **79,** 796–805 (2018).
27. Tamir, J. I., Ong, F., Cheng, J. Y., Uecker, M. & Lustig, M. Generalized magnetic resonance image reconstruction using the Berkeley Advanced Reconstruction Toolbox. In *ISMRM Workshop on Data Sampling & Image Reconstruction, Sedona, AZ* (2016).
28. Uecker, M. *et al.* Berkeley advanced reconstruction toolbox. *Proc. Intl. Soc. Mag. Reson. Med* **23,** 2486 (2015).
29. Zhang, T., Pauly, J. M., Vasanawala, S. S. & Lustig, M. Coil compression for accelerated imaging with Cartesian sampling. *Magn. Reson. Med.* **69,** 571–582 (2013).
30. Ben-Eliezer, N., Irani, M. & Frydman, L. Super-resolved spatially encoded single-scan 2D MRI. *Magn. Reson. Med.* **63,** 1594–1600 (2010).
31. Chen, L. *et al.* Super-resolved enhancing and edge deghosting (SEED) for spatiotemporally encoded single-shot MRI. *Med. Image Anal.* **23,** 1–14 (2015).
32. Chen, L. *et al.* An aliasing artifacts reducing approach with random undersampling for spatiotemporally encoded single-shot MRI. *J. Magn. Reson.* **237,** 115–124 (2013).
33. Seginer, A., Schmidt, R., Leftin, A., Solomon, E. & Frydman, L. Referenceless reconstruction of spatiotemporally encoded imaging data: principles and applications to real-time MRI. *Magn. Reson. Med.* **72,** 1687–1695 (2014).
34. Lustig, M., Donoho, D. L., Santos, J. M. & Pauly, J. M. Compressed Sensing MRI. *IEEE Signal Process. Mag.* **25,** 72–82 (2008).
35. Pruessmann, K. P., Weiger, M., Börnert, P. & Boesiger, P. Advances in sensitivity encoding with arbitrary k-space trajectories. *Magn. Reson. Med.* **46,** 638–651 (2001).
36. Block, K. T., Uecker, M. & Frahm, J. Undersampled radial MRI with multiple coils. Iterative image reconstruction using a total variation constraint. *Magn. Reson. Med.* **57,** 1086–1098 (2007).
37. Liu, B. *et al.* Regularized sensitivity encoding (SENSE) reconstruction using Bregman iterations. *Magn. Reson. Med.* **61,** 145–152 (2009).
38. Lustig, M., Donoho, D. & Pauly, J. M. Sparse MRI: The application of compressed sensing for rapid MR imaging. *Magn. Reson. Med.* **58,** 1182–1195 (2007).
39. Loris, I., Nolet, G., Daubechies, I. & Dahlen, F. A. Tomographic inversion using ℓ1-norm regularization of wavelet coefficients. *Geophysical Journal International* **170,** 359–370 (2007).

40. Kutyniok, G. Theory and applications of compressed sensing. *GAMM-Mitteilungen* **36,** 79–101 (2013).
41. Vauhkonen, M., Vadász, D., Karjalainen, P. A., Somersalo, E. & Kaipio, J. P. Tikhonov regularization and prior information in electrical impedance tomography. *IEEE Trans. Med. Imaging* **17,** 285–293 (1998).
42. Lukaschewitsch, M., Maass, P. & Pidcock, M. Tikhonov regularization for electrical impedance tomography on unbounded domains. *Inverse Problems* **19,** 585 (2003).
43. Ying, L., Xu, D. & Liang, Z.-P. On Tikhonov regularization for image reconstruction in parallel MRI. *Conf. Proc. IEEE Eng. Med. Biol. Soc.* **2,** 1056–1059 (2004).
44. Uecker, M. *et al.* ESPIRiT--an eigenvalue approach to autocalibrating parallel MRI: where SENSE meets GRAPPA. *Magn. Reson. Med.* **71,** 990–1001 (2014).
45. Solomon, E. *et al.* Overcoming limitations in diffusion-weighted MRI of breast by spatio-temporal encoding. *Magn. Reson. Med.* **73,** 2163–2173 (2015).
46. Solomon, E., Liberman, G., Nissan, N. & Frydman, L. Robust diffusion tensor imaging by spatiotemporal encoding: Principles and in vivo demonstrations. *Magn. Reson. Med.* **77,** 1124–1133 (2017).
47. Bottomley, P. A. & Hardy, C. J. Two-dimensional spatially selective spin inversion and spin-echo refocusing with a single nuclear magnetic resonance pulse. *J. Appl. Phys.* **62,** 4284 (1987).
48. Rieseberg, S., Frahm, J. & Finsterbusch, J. Two-dimensional spatially-selective RF excitation pulses in echo-planar imaging. *Magn. Reson. Med.* **47,** 1186–1193 (2002).

FIGURES

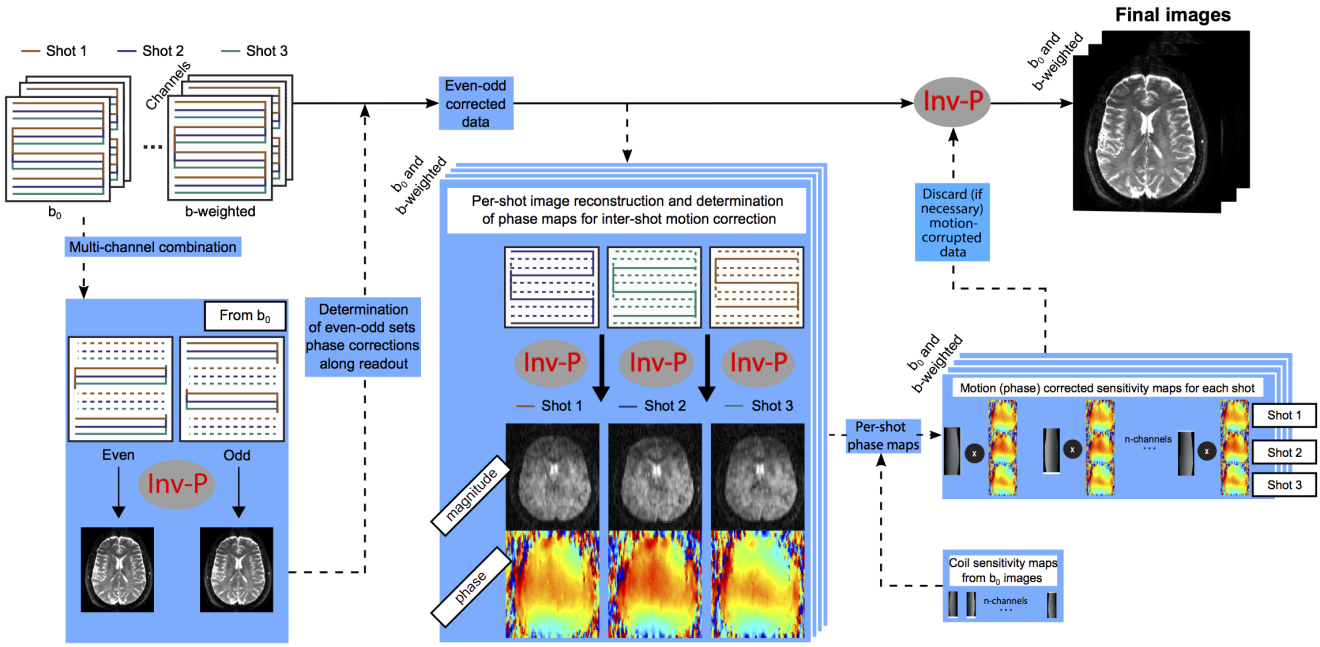

Figure 1: Processing principles of the interleaved, multi-shot SPEN MRI approach here introduced, as pertaining to a multi-b-value DWI acquisition relying on multiple parallel receivers. First, from each data set (i.e. each even or odd set, each diffusion-weighted data shot, or each repetition to be signal-averaged) a separate image is obtained. This operation (Inv-P) is performed using the l2-CG-ESPIRiT

algorithm, [27,28,44] based on an operator accounting for SPEN's quadratic phase encoding and for the sensitivity maps of the multiple coils. The method also considers the possibility of discarding a particular interleaved scan without resolution loss using information derived from multiple receivers (the SUSPENSE approach[26]) if motion-derived corruptions are detected. The final reconstruction follows the same path for every b-value (magenta), even if coil sensitivity maps are computed solely from the b_0 image.

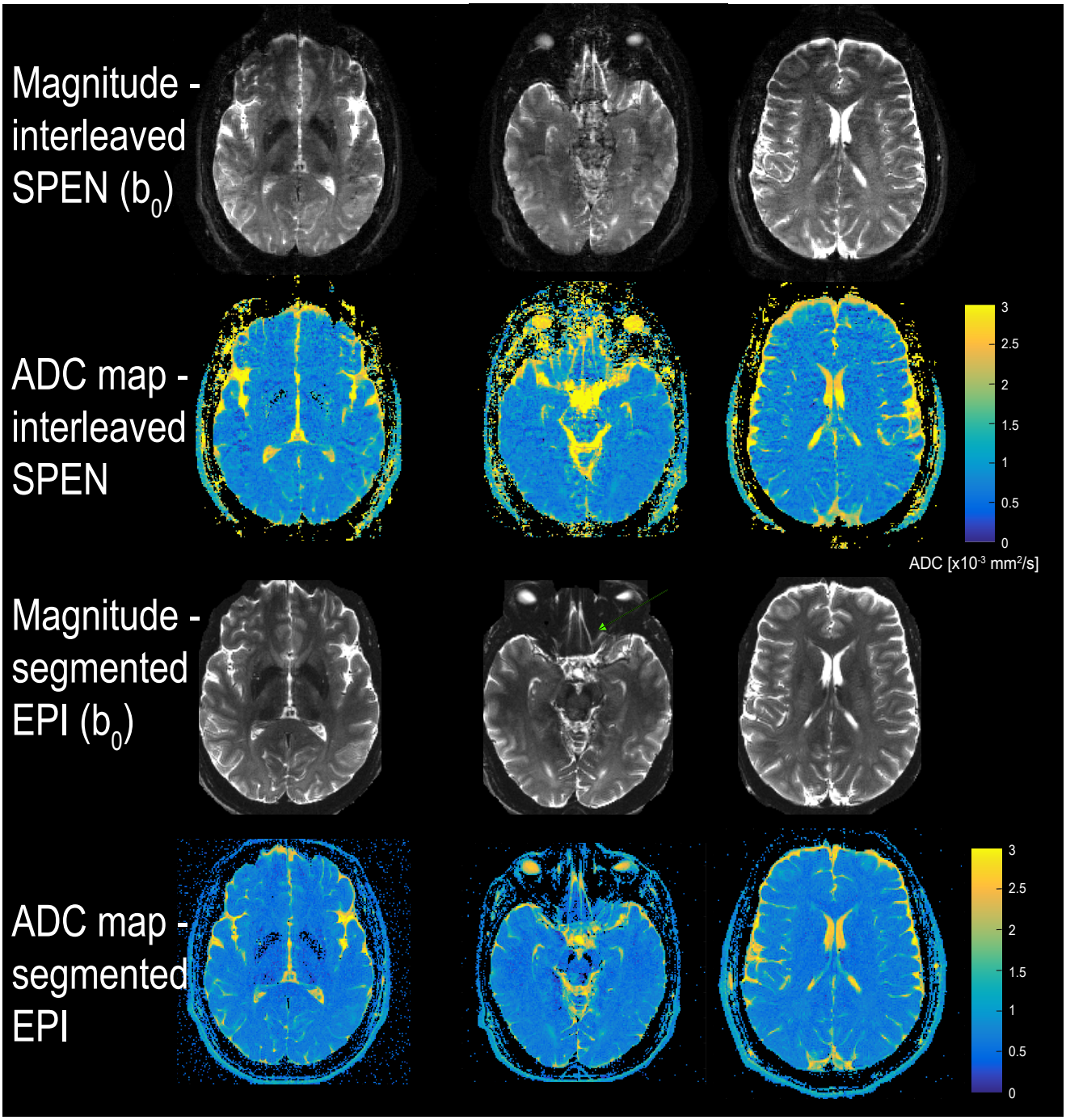

Figure 2: Comparison between representative SPEN slices acquired in eight shots and processed as described in Figure 1, against seven-segment EPI data collected with identical 1x1x3 mm resolutions. Shown are b_0 and ADC maps obtained by combining b_0 with orthogonal diffusion-weighted images;

notice the pile-up in the segmented EPI (green arrow), alleviated in SPEN. See Methods for additional details.

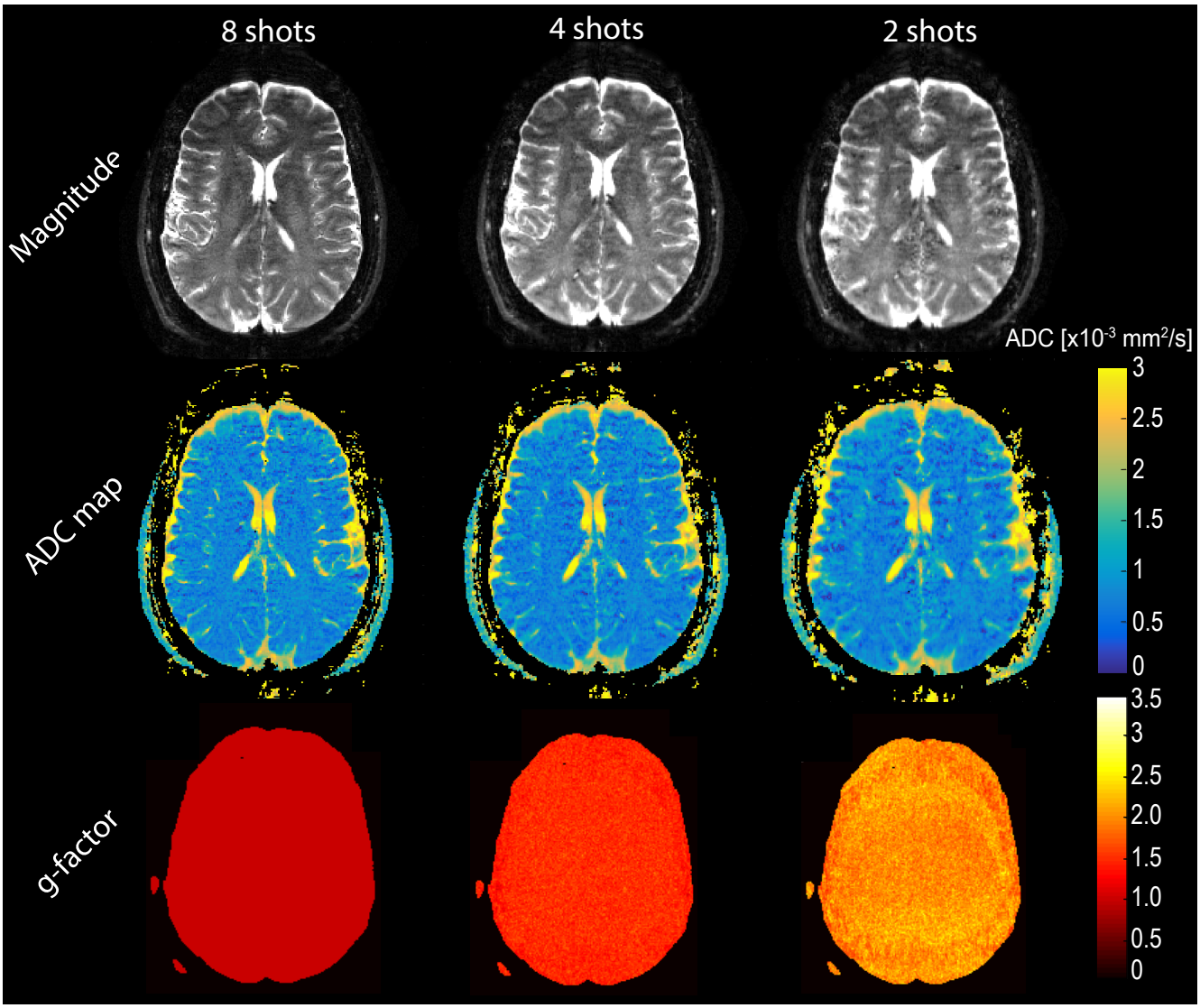

Figure 3: Comparison between the b_0, ADC maps and g-factor maps arising upon attempting to achieve the same data matrices using 8, 4 and 2 shots in the final reconstruction (g-factors were calculated by performing the reconstruction 100 times with 50% synthetic noise added to the data. These images were then used to obtain SNR as a ratio between mean intensity and its standard deviation on a pixel-by-pixel basis that was further used to calculate g-factors). Note that g-maps were calculated from images reconstructed to the same spatial resolution as the reference (i.e., to the eight-shots image) in order to evaluate noise amplification. In this instance the same l2 regularization (weighting multiplier 0.05) was used for the b_0 images and for the diffusion-weighted data. The impact of using different l2 weights on the ensuing spatial resolution achieved for various number of shots is examined in the Supporting Information (Supporting Information Figure S5).

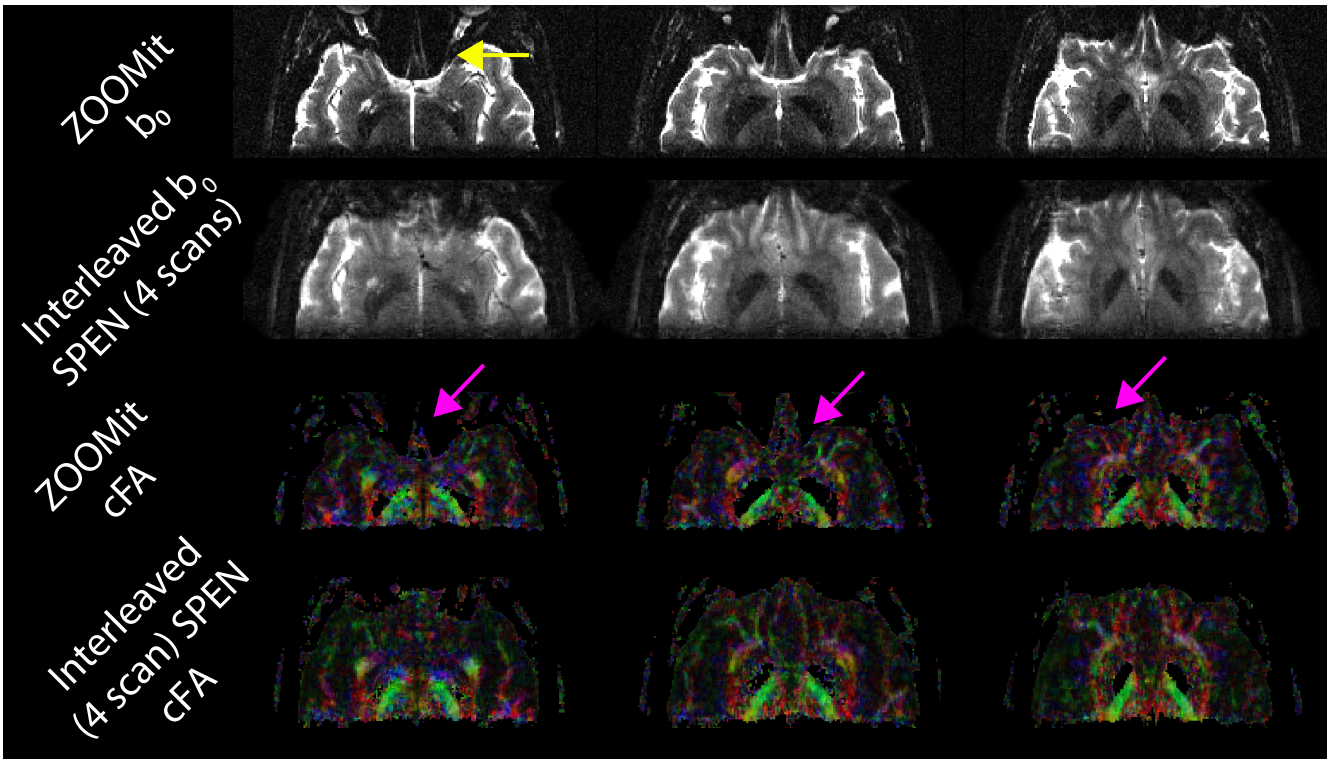

Figure 4: Comparison of b_0 and of fractional anisotropy (FA) maps arising from multiple restricted-FOV slices, targeting a human chiasma. ZOOMit experiments used a 2D-pulse and an EPI-based scheme; SPEN data resulted from four interleaved scans processed with the reconstruction introduced in Fig. 1. The yellow arrow highlights an optic nerve folded in the region of interest; magenta arrows show regions improved by the SPEN acquisition.

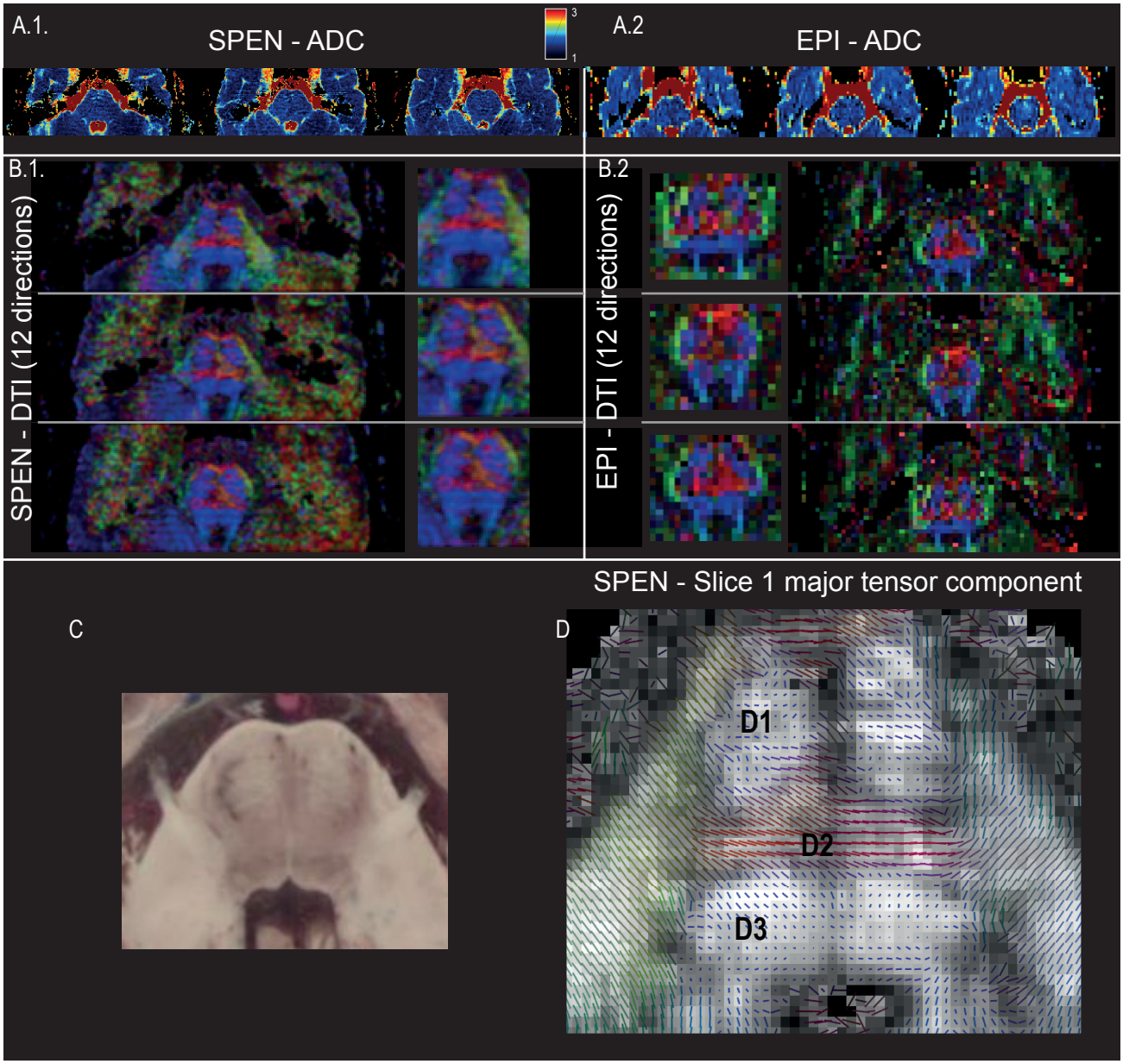

Figure 5: (A) Comparison of the ADC maps obtained with DTI SPEN (A.1, 0.74x0.74 mm in plane resolution) and DTI EPI (A.2, 2x2 mm in plane resolution) for three representative slices located in the pons region. (B) DTI data recorded using 12 directions for both SPEN (B1) and EPI (B2). (C) Anatomical slice highlighting the region of interest in these studies (taken from http://brainmaps.org/), corresponding to the zoomed DTI maps in panels B.1, B.2. (D) Main FA components revealed by the SPEN measurement for a similar slice, pointing out different anatomical parts (see text for details).